Atomic-Scale Observation of the Local Structure and 1D Quantum Effects in vdW Stacking Mo_6Te_6 Nanowires

Yuang Li, Di Wu, Dongli Wang, Yinuo Zhang, Tai Min, and Yi Pan*

The sub-nanometer-diameter transitional-metal chalcogenides (M_6X_6) molecular wires are ideal 1D quantum systems. The electronic properties of such system are very sensitive to the interface interaction and local imperfection. Here, the atomic structure and local electronic structure of van der Waals (vdW) stacking Mo_6Te_6 nanowires fabricated by using molecular beam epitaxy are reported. Atomic-resolution scanning tunneling microscopy measurement shows that the vdW interface distance varies from 0.71 to 1.05 nm when Mo_6Te_6 wires stacked on graphite, $MoTe_2$, and Mo_6Te_6 surfaces. Scanning tunneling spectroscopy confirmed the 1D quantum effect of van Hove singularity and Tomonaga–Luttinger liquid behavior at 77.8 K. Single Te vacancies and their effect to the local structure distortion are observed as well. These observations shed light on the local structure and quantum effects of the M_6X_6 nanowire materials, which may find applications in future electronic devices.

1. Introduction

In recent years, 1D van der Waals (vdW) materials have attracted increasing attention due the intriguing quantum confinement effects, magnetic and spintronic properties, as well as the potential application in electronics.[1] As a member of the 1D vdW materials, the transition metal chalcogenides M_6X_6 (M = Mo, W; X = S, Se, Te) could easily disperse into single wire with a diameter below 1 nm. Thus, it was considered as an ideal metallic 1D model system for exploring the unique quantum effect in low dimensional physics, e.g., van Hove singularity (VHS) in the density of state,[2] Tomonaga–Luttinger liquid (TLL) behavior in electron transport,[3] phason polarons on the 1D charge density wave (CDW) state.[4] The metallic M_6X_6 nanowires could directly bond to the semiconducting 2D MX_2 sheets and form defect-free metal–semiconductor heterostructure,[1d,5]

which opens up the potential application in all vdW materials-based integrated circuits. As a preliminary example, the Mo_6Te_6/$MoTe_2$ heterostructures have been used as electrode to improve the efficient of supercapacitors.[6] Due to the high capacity in the space between the vdW stacking M_6X_6 molecular wires, the metal ion-inserted M_6X_6 structures (Chevrel phases) could further expand its their application to superconductors[7] and ion batteries.[8]

The nanowires and nanowire bundles are mechanically flexible due to the 1D covalent framework and vdW interaction that allows slipping of single wires against each other. Atomic force microscope measurement shows that Mo_6Se_6 single wires could be highly curved in nanometer scale while maintaining micrometer scale length.[2a] Ab initio calculations indicate that the M_6X_6 wires are stiff along the axis with the elastic constant higher than steel,[9] while flexible radially with the electronic transport property unaffected by the bending.[10] The structure flexibility is also facilitated by forming axial kinks, rotational twists, and branches.[1d,5a]

Recently, more intriguing properties have been predicted by first principles calculations. Jin et al. reported that in a periodically doped M_6X_6 1D wire, the system could be depicted by extended Su-Schrieffer-Heeger (SSH) model, and thus the topological nontrivial edge modes with $e/2$ fractional charges would exist.[11] Shang et al. calculated 66 nanowires of 3d, 4d, and 5d transition metal chalcogenides in the M_6X_6 stoichiometry and predicted that Co- and Fe-based M_6X_6 to be robust ferromagnets with Curie temperature up to 700 K.[12]

The Mo-Te binary system is particularly suitable for research since tuning between the various phases is highly feasible.[13] Although the structure and electronic properties of free standing and epitaxial nanowires have been explored by using microscopic methods,[2b,3–5] the atomic-scale investigations that elucidating the staking dependent local structure and electronic of Mo_6Te_6 wires are still lacking.

In this paper, we report the atomic structure and local electronic structure of Mo_6Te_6 molecular wires stacking on varying vdW surfaces, including highly oriented pyrolytic graphite (HOPG), $MoTe_2$, and Mo_6Te_6 array. The pristine and defective Mo_6Te_6 wires are synthesized by using molecular beam epitaxy (MBE). Low-temperature scanning tunneling microscope (STM) and spectroscopy measurement reveals the influence of the interface interaction to the structure and local electronic structure, e.g., VHSs in

Y. Li, D. Wu, D. Wang, Y. Zhang, T. Min, Y. Pan
Center for Spintronics and Quantum Systems
State Key Laboratory for Mechanical Behavior of Materials
Xi'an Jiaotong University
Xi'an 710049, China
E-mail: yi.pan@xjtu.edu.cn

**ADVANCED
SCIENCE NEWS**

www.advancedsciencenews.com

**ADVANCED
MATERIALS
INTERFACES**

www.advmatinterfaces.de

the density of states and TLL behavior at 77.8 K. Additionally, single Te vacancies and the induced defect states and local structure distortion are discussed. This work shed light on the stacking dependent quantum effects of 1D nanowires.

2. Results and Discussion

2.1. Formation of Mo_6Te_6 Nanowires Stacking on Different Surfaces

The binary transition metal chalcogenides M_6X_6 phase is molecular crystal like vdW stacking nanowire bundles. We employ the strategy of vacuum annealing of the epitaxial $MoTe_2$ ultrathin films to fabricate the Mo_6Te_6 nanowire (MTNW) samples, as described in the Experimental Section. During the high-temperature postannealing of $MoTe_2$ in ultra-high vacuum (UHV), lattice Te atoms gradually dissociate from the film by forming vacancies and mirror twin boundaries, thus the Mo:Te atom ratio could be well tuned by annealing temperature and holding time. When the local stoichiometric ratio reached 1:1, the Mo_6Te_6 phase starts to nucleate and grow. Such a transition could be very fast for the atomically thin film when the temperature is above 870 K, resulting in the rough Mo_6Te_6 bundle network unsuitable for detailed STM investigation. In order to study the early-stage growth of Mo_6Te_6 nanowire and their stacking on different surface, we optimized the annealing parameters and preserved a multiphase coexisting sample with 1D Mo_6Te_6 and 2D $MoTe_2$ by fast cooling after moderate temperature annealing at 720 ± 1 K. The overview topographic STM image confirmed the formation of chain-shaped Mo_6Te_6 on the 2D $MoTe_2$ islands, as shown in **Figure** 1A. The zoomed-in STM image (Figure 1B) further reveals that the Mo_6Te_6 nanowires are actually lying on different surfaces. To better illustrate these structures, a schematic map is shown in Figure 1C, corresponding to the STM images in Figure 1B. The gray and orange areas indicate the HOPG substrate and the $MoTe_2$ islands, respectively. To distinguish the morphologies of MTNWs stacking on different surfaces, the single-layer MTNWs that parallelly arranged on HOPG are indicated by light green areas, which we defined as Mo_6Te_6 array. The MTNWs stacking on the Mo_6Te_6 array or $MoTe_2$ islands are indicated by blue rectangles, which are refer to Mo_6Te_6 bundles. By comparing Figure 1B,C, one can easily distinguish the three different stacking types of nanowires.

The STM image in Figure 1D shows the lateral heterostructure of Mo_6Te_6 array inserted into monolayer $MoTe_2$ island, which provides a snapshot of early-stage transformation from $MoTe_2$ to MTNWs. It implies that the MTNWs initially formed at the edges of $MoTe_2$ island, and then spread into the inner region of island by forming parallel arrays directly stacking on HOPG substrate (see time-dependent annealing results in Figure S4, Supporting Information). Figure 1E shows the atomic-resolution image zoomed-into the region in Figure 1D, indicated by white dashed frame, where the units of the single NTNW can be resolved. According to the crystal structure of Mo_6Te_6, each unit contains six inner Mo and six outer Te atoms, as displayed in Figure 1F. By measuring the line profile curves plotted in Figure 1G, which were taken along the lines of corresponding color in Figure 1D,E, we obtained that the

unit-distance within the wire and lateral space between the wires in the array is 4.6 and 8.1 Å, respectively.

The second-layer MTNWs are grown on top of the MTNW array or monolayer $MoTe_2$ island, as shown in Figure 1H,I, respectively. When they are stacking on the Mo_6Te_6 array and forming double-layer MTNW bundle, the second-layer nanowires are very straight and highly oriented due to confining effect of the array below. On the other hand, MTNWs stacking on $MoTe_2$ could be curved, exhibiting their flexibility.

Based on a height profile analysis upon STM images, we obtained the measured lateral wire–wire distance (D_{w-w}) and vertical wire–surface distance (D_{w-s}) on different surfaces (seen in Figures S1 and S2, Supporting Information). Generally, the D_{w-w} is varying in a small range between 8.1 and 8.9 Å (seen in Table S1, Supporting Information). When the MTNWs were formed inside the $MoTe_2$ island during growth, the ends of MTNW were anchored to the $MoTe_2$ lattice, thus D_{w-w} is a short (8.1 Å), as in the case shown in Figure 1E. When the transformation is finished and the MTNWs form an array, the D_{w-w} is balanced at a larger value 8.7Å. It is worth noting that the D_{w-w} within the second-layer MTNWs that stacking on Mo_6Te_6 array expands to 8.9 Å, in good agreement with the value in the bulk Mo_6Te_6 crystal.

The height of the MTNW is also varying when they are stacking on different surfaces, thus we can evaluate the wire–surface distance D_{w-s} by comparing the height. The D_{w-s} are varying in a large range from 7.1 to 10.5 Å on different surfaces, which indicate sensitive-stacking dependency. In Figure 1J, the orange, red, and green curves plot the height profile along the corresponding lines in Figure 1D,H,I. We also conducted the same measurement within one STM overview images to eliminate the accidental error (seen in Figure S2, Supporting Information). The height profiles show that the apparent height of MTNWs is 10.5 and 9 Å when they are stacking on HOPG and $MoTe_2$. Such difference implies that MTNWs are more loosely bond to HOPG substrate comparing with $MoTe_2$ substrate. In the double-layer stacking MTNWs, the height of top layer nanowires on Mo_6Te_6 array is only 7.1 Å, since they lie in the trench between underlayer array, which implies the MTNWs within the multilayer are bonded stronger than that those lying on the flat vdW surfaces.

The MTNWs stacking on different surfaces exhibit varying lateral wire–wire distances and vertical wire–surface heights, as well as apparent morphological defferences. We attribute these differences to the surface corrugation and confining effect of different surfaces to the MTNWs. The HOPG is a super flat substrate that provides less constrain to the MTNWs, giving rise to larger space between wires. The Mo_6Te_6 array is corrugated substrate, which provides strong constrain to the wires on top, so the wires are very straight and regular. The $MoTe_2$ is a flat substrate providing intermediate constrain, which allows bending of the wires. The influence of the van der Waals substrates to the nanowire would provide method to tune the structure of nanowire in the devices.

2.2. Isolated Mo_6Te_6 Nanowires

The isolated double wire on the Mo_6Te_6 array is shown in the top-view 3D STM image in **Figure** 2A. These wires are straight

2202043 (2 of 8)

**ADVANCED
SCIENCE NEWS**

www.advancedsciencenews.com

**ADVANCED
MATERIALS
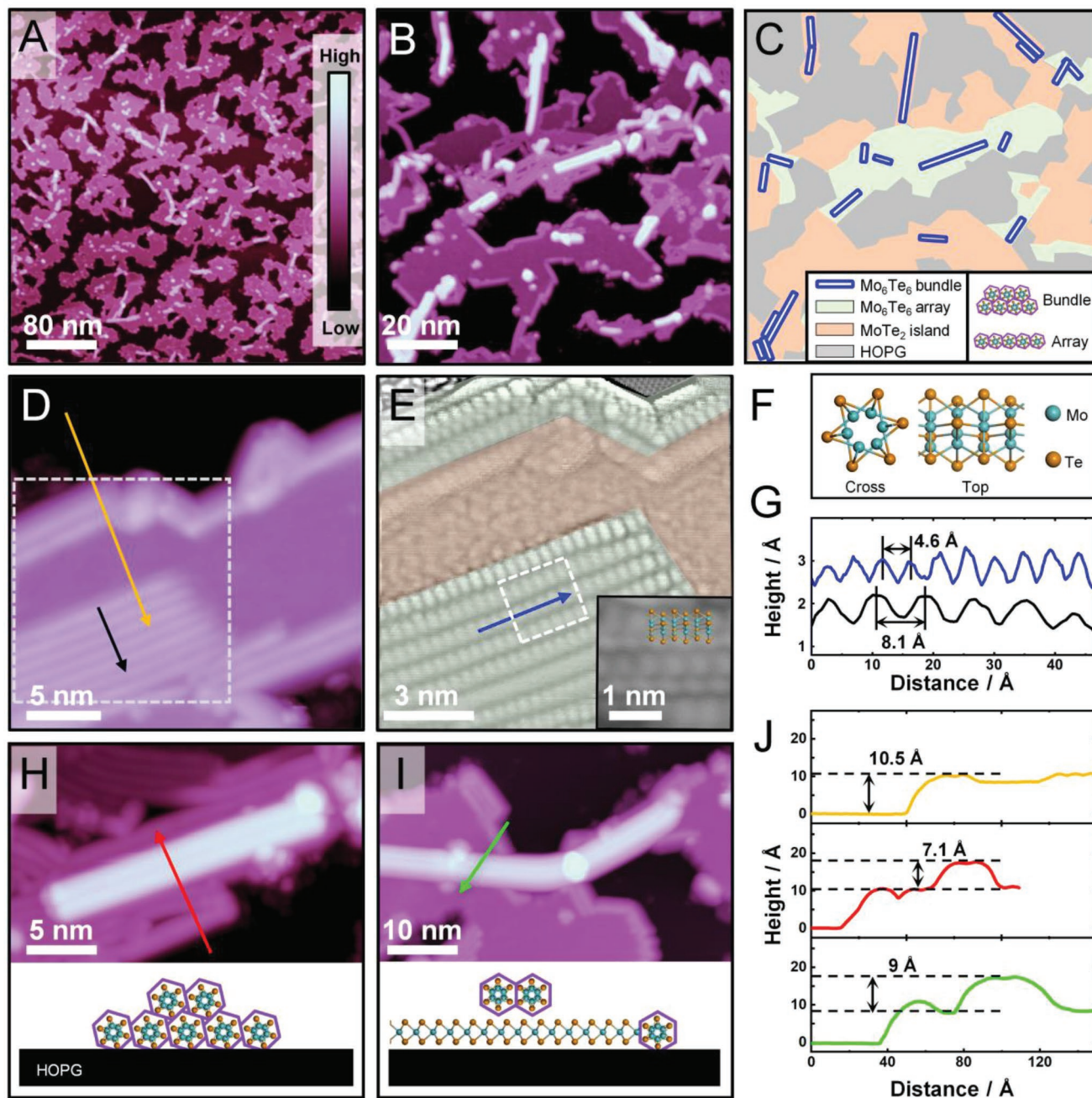INTERFACES**

www.advmatinterfaces.de

Figure 1. Mo_6Te_6 nanowires (MTNW) stacking on different surfaces: A) Overview STM image of the MTNW sample prepared by vacuum annealing of $MoTe_2$ ($V_b = 2$ V, $I_t = 20$ pA). B) Zoomed-in STM image showing coexistence of $MoTe_2$ and Mo_6Te_6 ($V_b = -2$ V, $I_t = 20$ pA). C) Schematic map extracted from (B) to distinguish different regions. D) STM image of $MoTe_2$ island with Mo_6Te_6 array ($V_b = -2$ V, $I_t = 30$ pA). E) Zoomed-in image of the area enclosed by the white line box in (D) ($V_b = -1$ V, $I_t = 100$ pA); inset: atomic resolution of Mo_6Te_6 wire in the dashed white line box in (E) ($V_b = 0.2$ V, $I_t = 100$ pA). F) Ball-stick structure model of Mo_6Te_6 nanowire. G) Line profiles along the black and blue lines in (D) and (E), respectively. H) isolated wires on MTNW array ($V_b = -2$ V, $I_t = 50$ pA) and the schematic of stacking configuration. I) isolated wires on $MoTe_2$ island ($V_b = -2$ V, $I_t = 20$ pA) and the schematic stacking configuration. J) Height profiles taken along lines of corresponding color in (D), (H), and (I).

and regular, and the top rows of Te atoms are clearly resolved. Additionally, all of the three rows of exposed outer Te atoms can be seen in the side view of the same structure, as indicated by the three arrows in Figure 2B. A zoomed-in image of the double wire in Figure 2C reveals that the top-layer wire is lying in between two wires below, thus forms a close-packed

nanowire bundle as depicted by the structure ball-stick model, which is in good agreement with the transmission electron microscope (TEM) cross-section image of the MTNW crystal.[13a] Interestingly, when the line profile across the top-layer MTNWs (as marked by the red line in Figure 2C) is compared with that across the Mo_6Te_6 array below (as marked by the blue line), it is
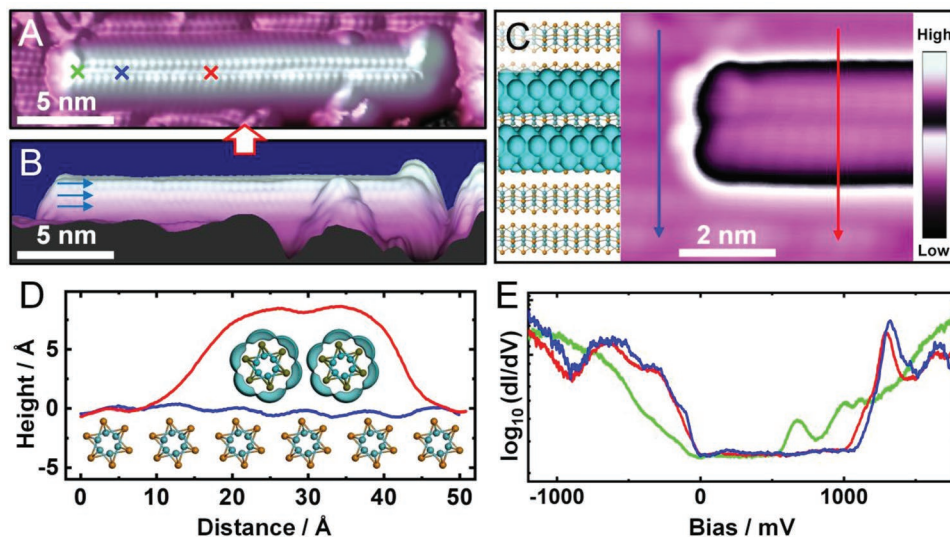
**ADVANCED
SCIENCE NEWS**

www.advancedsciencenews.com

**ADVANCED
MATERIALS
INTERFACES**

www.advmatinterfaces.de

Figure 2. Atomic structure and local electronic structure of isolated Mo_6Te_6 nanowires: A) Top view and B) side view of 3D STM image of the double wire ($V_b = -0.5$ V, $I_t = 100$ pA). C) Structure model and zoom-in image at the end the wires ($V_b = -0.5$ V, $I_t = 100$ pA). D) Height profiles along lines of corresponding color in (C), with inserted cross section view of the model. E) Scanning tunneling spectra acquired at the positions marked by crosses in correspond color in (A) ($V_{mod} = 7.07$ mV$_{rms}$).

clearly seen that the distance 8.9Å between the top layer is obviously larger than that in the array (8.4Å), as shown in Figure 2D. This implies the isolated wires on the surface experience an expanding relaxation. We attribute this effect to the reduced confining of vdW interaction from less nearest neighbors.

The local electronic properties of the 1D MTNW were investigated by conducting scanning tunneling spectroscopy (STS) measurement on the wires. The single-point STS spectra taken at different spots on the wire, as marked by the green, blue, and red crosses, are plotted in corresponding color in Figure 2E. The blue and red spectra display the intrinsic local electronic structure of the 1D wires. Below the E_F, the conductance is high with multiple broad peaks, revealing the obvious metallicity of the 1D wires. From E_F to about 1 V, there is low but non-zero conductance region. Zoom-in STS spectra with short tip-sample distance reveals detectable density of state in this region (Figure S3, Supporting Information), which confirms that the nanowires are metallic, in consistent with STS results on similar Mo_6Se_6 nanowires.[4] Interestingly, very sharp peaks appear at 1.32 and 1.65 V. We attribute the sharp peaks to van Hove singularities in the density of state, which is consistent with the previous work on the Mo_6Se_6 nanowires on HOPG substrate.[2a] Additionally, STS taken at the end of wire (green curve) shows that the VHS states disappears, while new in-gap states arise. The disappearance of VHS states is most likely due to the vanishing of 1D characteristic at the end of the wire. These new states might have trivil origion of dangling bonds. Jin et al. predicted the topological end state would appear in such transition metal chalcogenides nanowires when dimerization occurs and the electronic structure of the system can be described by the SSH model.[11] Thus, it would interesting to induce dimerization via interface interaction by choosing the substrate with suitable lattice constant. Exploration of that would be very important, yet requires further study in the future.

2.3. Mo_6Te_6 Nanowire Array on HOPG

To investigate the atomic structure and local electronic structure of each MTNW within the array, we focus on an isolated and fully developed Mo_6Te_6 array, as shown in **Figure 3**A. The MTNWs are oriented in three equivalent orientations parallel to the [001] direction of HOPG substrate. The atomic resolution image of the region enclosed in the yellow-dashed frame is shown in Figure 3B, where the peculiar morphology of each wire is clearly resolved. For the out-most nanowire at the right edge, three rows of Te atoms in the wire are clearly seen. But for the second wires, only two rows of Te atom are seen, since the lower row is blocked by the neighboring wire.

Such atomic-resolution images allow us to evaluate the rotation and twist within a single MTNW. Focusing on the outermost wire in Figure 3B, the right row of Te atoms is lower than the other two rows, which means they are lower and confirm the axial rotation of single wire as in the bulk MTNW crystals. For the Te atom along the wire, the height remains constant in the same rows, indicating there is no axial twist along the wire. Comparatively, an axial twist within the wire can be observed in the inner third to fifth wires. The height profile along the red line crossing six MTNWs is plotted in Figure 3C. It shows that the D_{w-w} is larger for the outer wire, but D_{w-s} is higher for the inner wires. Thus, we can interpret the local twist is originated from spontaneous adaption to the smaller space between wires. These results might elucidate the mechanism of astonishing flexibility of the vdW-stacking nanowires.

In order to further investigate the influence of twist to local electronic structure, we took a series of STS on the twisted wire, as shown in Figure 3D. The positions of STS are indicated by crosses in the image inserted, which clearly displays that the twist mainly occurs at the black cross, where a twist angle of 11° can be estimated (see Figure S5, Supporting Information). The corresponding black curve of STS shows new peaks
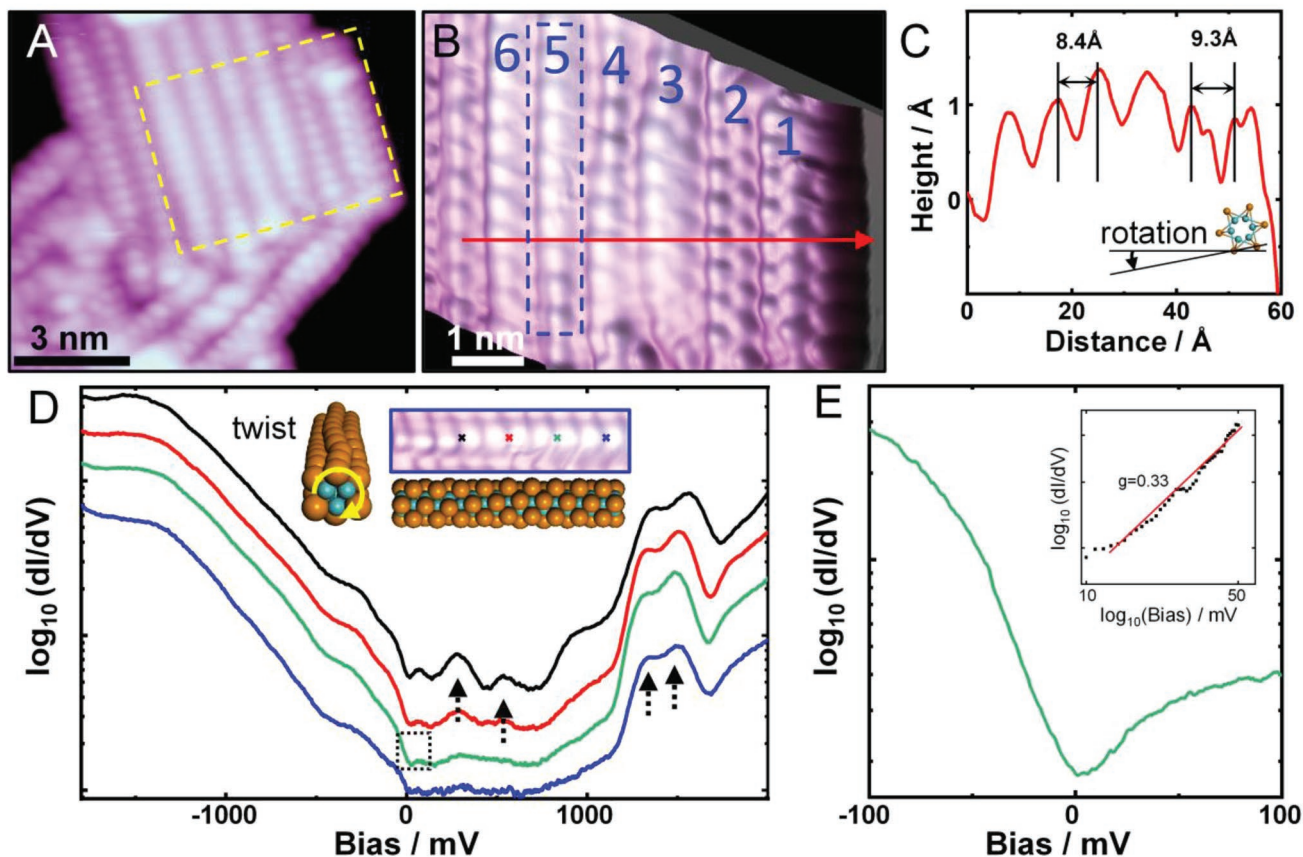
Figure 3. Mo_6Te_6 nanowires array on HOPG surface: A) High-resolution STM image of a nanowire array (V_b = 0.5 V, I_t = 100 pA). B) 3D STM image in the area enclosed in yellow-dashed line box in (A) (V_b = −0.1 V, I_t = 100 pA). C) Height profile along red line in (B). Insert: Axial rotation is indicated. D) Scanning tunneling spectra acquired on different positions of the locally twisted wire, as marked by the crosses in corresponding color (V_{mod} = 17.67 mV_{rms}). The spectra are offset vertically for clarity. Inset: zoom-in image of the twisted Mo_6Te_6 wire in the blue-dashed line box in (B); the side view and top view structure model of the twisted wire. E) STS acquired at the green cross-position, in smaller energy range (V_{mod} = 7.07 mV_{rms}). Inset: A double logarithmic plot of spectrum within the energy range of bias 10–50 mV.

around E_F, e.g., the one at 280 mV. Since there is no defect or impurity around, the defect induced in-gap states can be ruled out. Thus, we can attribute these states to the VHS peaks arising from local twist. When the twist occurs within a nanowire, both the intensity and position of the VHS peaks could be affected. Such twist induced VHS states variation had been predicted by Popov et al. in a theoretical study,[10] which agrees well with our observation. Except for the new peaks, the spectra in Figure 3D generally show the nonzero density of states in a wide bias range between ±2 V, revealing that the wires in the array are metallic. Interestingly, the VHS peaks on the Mo_6Te_6 array are broadened comparing with that on the isolated wires (Figure 2E). This implies the suppression of 1D characteristics by HOPG substrate. Earlier studies also reported the suppression of VHS on HOPG.[2a]

Note that spectra in Figure 3D reveal a small dip around E_F energy, we thus conducted the single-point STS spectrum over a smaller energy range at the position of green cross, as shown in Figure 3E. The curve shows a power-law line shape, which is actually due to the TLL behavior of e–e interaction in the 1D metallic system. Such phenomenon previously has been observed in STS spectra obtained on the W_6Te_6 nanowires.[3b]

From the linear fitting to double logarithmic plot of dI/dV within energy range of ±50 mV, as shown in the inset, the Luttinger parameter g of 0.33 was extracted, indicating the strong e–e interaction is playing an important role in electron transport at 77.8 K.

2.4. Defects in Mo_6Te_6 Wires

Apart from the highly ordered pristine MTNWs, defective MTNWs are occasionally observed, mostly on the $MoTe_2$ surface. **Figure 4**A–D displays the bias-dependent topographic STM images of the defective Mo_6Te_6 bundle composed of three single wires. At the tunneling bias of 2 V, the image shows homogeneous wires, which are obviously curved comparing with the straight one in Figure 3A. While the tip-sample distance decrease with reducing bias, more local features are resolved. In the empty-state image (Figure 4B, V_b = 1 V) and filled-state image (Figure 4C, V_b = −0.2 V), protrusion and depression are observed in the corresponding spots, respectively. Figure 4D shows an atomic-resolution image obtained with superior sharp tip due to accident modified, which
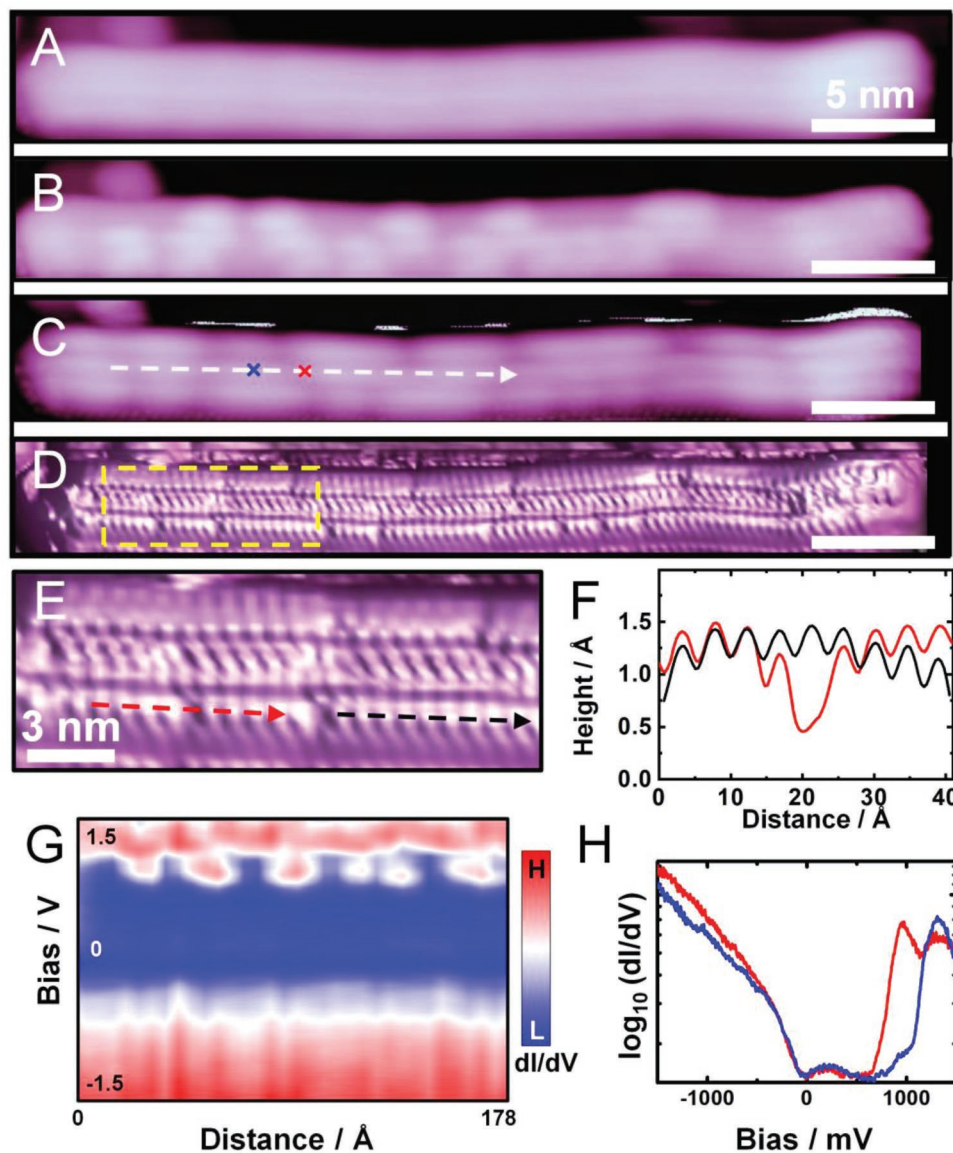
**ADVANCED
SCIENCE NEWS**

www.advancedsciencenews.com

**ADVANCED
MATERIALS
INTERFACES**

www.advmatinterfaces.de

Figure 4. Te vacancy defects in the Mo_6Te_6 nanowires: A–D) Series of STM images acquired at a series V_b of 2, 1, –0.2, and 0.5 V, respectively ($I_t = 100$ pA). D) is illustrated in 3D for clarity. E) Zoom-in image of the area in the yellow-dashed line box in (D). F) Height profiles along red- and black-dashed lines in (E) showing the single Te vacancy. G) 2D plot of 35 scanning tunneling spectra along the white-dashed line in (C) ($V_{mod} = 7.07$ mV_{rms}). H) STS spectra acquired at positions on and off a single vacancy, as indicated by the crosses in (C) ($V_{mod} = 7.07$ mV_{rms}).

reveals that the fine features are originated from defects in the wires. The zoom-in image in Figure 4E and line profile curves in Figure 4F reveal that such defects are actually single Te vacancies.

To further investigate the influence of defects to local electronic structure, 35 STS spectra were taken along the white-dashed line in Figure 4C. The representative single-point STS spectra on the defect (marked by red cross) and regular spot (marked by blue cross) are shown in Figure 4H, which reveals the defect-induced new state at 962 mV. However, the 1D characteristics dip at E_F remain intact. A 2D plot of all 35 spectra in Figure 4G confirmed that the states are highly localized around the defects. Thus, we anticipate such

defects are largely unharmful to the transport properties of the MTNW.

Similar chalcogen atom vacancies in the M_6X_6 wires have be created by electron beam radiation in TEM. Interestingly, it was found the chalcogen vacancy could facilitate the bending by reducing the deformation energy, while maintaining the metallicity of the wires.[5a] This is in good consistence with our observation. We assume the defect are formed due to local Te deficiency under the high-temperature vacuum annealing process. They are playing important roles in the superior flexibility of such inorganic molecular nanowires. Additionally, the single vacancies with in-gap states might find application in quantum devices as charge/spin trap.

**ADVANCED
SCIENCE NEWS**

www.advancedsciencenews.com

**ADVANCED
MATERIALS
INTERFACES**

www.advmatinterfaces.de

3. Conclusion

In conclusion, we have synthesized Mo_6Te_6 nanowires stacking on different vdW surfaces, including HOPG, monolayer $MoTe_2$, and Mo_6Te_6 array, by vacuum annealing and quick cooling of MBE grown $MoTe_2$. Low-temperature STM and STS measurement reveals that the atomic structure and electronic structure could be tuned by the interface vdW interaction with the surface they stack on. On the HOPG surface, the MTNWs form parallel aligned arrays, but single wires have more freedom to relax by adapting the space, rotation angle or even twist within the same wire. The dI/dV spectra confirm the metallic electronic structure and TLL behavior. On the Mo_6Te_6 array, the top layer wires are in more regular shape and exhibiting sharper VHS peaks in the dI/dV spectra, implying the pristine 1D structure and electronic structure characteristics. On monolayer $MoTe_2$ surface, the MTNWs often show curved feature that was accompanied by the Te vacancies. Such vacancies could induce highly localized in-gap states, but did not disturb the TLL behavior around E_F. Our findings shed light on the atomic details of the flexibility and robust 1D electronic properties in the transition metal chalcogenides 1D vdW materials, which might find important application in nanoscale quantum devices in the future.

4. Experimental Section

Sample Preparations: Epitaxial 1–2 layer $MoTe_2$ films were grown on HOPG substrate in a UHV MBE system equipped with quatz crystal microbanlence (QCM) and reflecrtion high-energy electron diffraction (RHEED). High-purity Te (99.999%, Alfa Aesar) and Mo (99.95%, Alfa Aesar) were coevaporated by standard K-cell and E-beam evaporator, respectively. During the deposition, the Te/Mo flux ratio was kept at 10:1, while the substrate temperature was maintained at 620 ± 2 K. The thickness of the film was controlled by tuning growth time and calibrated by using QCM. The Mo_6Te_6 nanowire samples were synthesized by vacuum annealing of as-prepared $MoTe_2$ thin films. It was conducted by prolonged annealing for 60 min at 720 ± 1 K in situ, with the background pressure lower than 5E-10 mbar. The sample was then quickly cooled down to 200 K on cold stage within 5 min. After that, the as-grown sample was immediately transferred to a custom-made cryogenic STM (Createc).

STM/STS Measurements: The characterization was performed at 77.8 K using a electrochemically etched W tip. The tunneling spectra were obtained by using lock-in technique with 5–20 mV AC modulation voltage at 833 Hz.

Supporting Information

Supporting Information is available from the Wiley Online Library or from the author.

Acknowledgements

Conflict of Interest

The authors declare no conflict of interest.

Data Availability Statement

The data that support the findings of this study are available from the corresponding author upon reasonable request.

Keywords

[1] a) H. Song, T. Li, J. Zhang, Y. Zhou, J. Luo, C. Chen, B. Yang, C. Ge, Y. Wu, J. Tang, *Adv. Mater.* **2017**, *29*, 1700441; b) L. Du, Y. Zhao, L. Wu, X. Hu, L. Yao, Y. Wang, X. Bai, Y. Dai, J. Qiao, M. G. Uddin, X. Li, J. Lahtinen, X. Bai, G. Zhang, W. Ji, Z. Sun, *Nat. Commun.* **2021**, *12*, 4822; c) Y. C. Du, G. Qiu, Y. X. Wang, M. W. Si, X. F. Xu, W. Z. Wu, P. D. D. Ye, *Nano Lett.* **2017**, *17*, 3965; d) J. Lin, O. Cretu, W. Zhou, K. Suenaga, D. Prasai, K. I. Bolotin, N. T. Cuong, M. Otani, S. Okada, A. R. Lupini, J.-C. Idrobo, D. Caudel, A. Burger, N. J. Ghimire, J. Yan, D. G. Mandrus, S. J. Pennycook, S. T. Pantelides, *Nat. Nanotechnol.* **2014**, *9*, 436.

[2] a) L. Venkataraman, C. M. Lieber, *Phys. Rev. Lett.* **1999**, *83*, 5334; b) J. Kibsgaard, A. Tuxen, M. Levisen, E. Laegsgaard, S. Gemming, G. Seifert, J. V. Lauritsen, F. Besenbacher, *Nano Lett.* **2008**, *8*, 3928.

[3] a) L. Venkataraman, Y. S. Hong, P. Kim, *Phys. Rev. Lett.* **2006**, *96*, 076601; b) Deng, D. H. , Y. Bai, Y. Guo, Z. Pan, S. Lu, P. Cui, Z. Zhang, C. Zhang, *Nano Lett.* **2020**, *20*, 8866; c) Y. Xia, B. Wang, J. Zhang, Y. Jin, H. Tian, W. Ho, H. Xu, C. Jin, M. Xie, *Nano Lett.* **2020**, *20*, 2094.

[4] X. Yang, J.-J. Xian, G. Li, N. Nagaosa, W.-H. Zhang, L. Qin, Z.-M. Zhang, J.-T. Lü, Y.-S. Fu, *Phys. Rev. X* **2020**, *10*, 031061.

[5] a) J. Lin, Y. Zhang, W. Zhou, S. T. Pantelides, *ACS Nano* **2016**, *10*, 2782; b) Y. Y. Yu, G. Wang, Y. Tan, N. N. Wu, X. A. Zhang, S. Q. Qin, *Nano Lett.* **2018**, *18*, 675.

[6] S. A. Pawar, D. Kim, R. Lee, S. W. Kang, D. S. Patil, T. W. Kim, J. C. Shin, *Chem. Eng. J.* **2019**, *371*, 182.

[7] a) A. P. Petrovic, D. Ansermet, D. Chernyshov, M. Hoesch, D. Salloum, P. Gougeon, M. Potel, L. Boeri, C. Panagopoulos, *Nat. Commun.* **2016**, *7*, 12262; b) D. Ansermet, A. P. Petrovic, S. He, D. Chernyshov, M. Hoesch, D. Salloum, P. Gougeon, M. Potel, L. Boeri, O. K. Andersen, C. Panagopoulos, *ACS Nano* **2016**, *10*, 515; c) A. P. Petrovic, R. Lortz, G. Santi, M. Decroux, H. Monnard, O. Fischer, L. Boeri, O. K. Andersen, J. Kortus, D. Salloum, P. Gougeon, M. Potel, *Phys. Rev. B* **2010**, *82*, 235128.

[8] a) J. M. Tarascon, *J. Electrochem. Soc.* **1985**, *132*, 2089; b) J. M. Tarascon, *Mater. Lett.* **1985**, *3*, 375; c) P. S. E. Yeo, M.-F. Ng, *Chem. Mater.* **2015**, *27*, 5878.

[9] F. J. Ribeiro, D. J. Roundy, M. L. Cohen, *Phys. Rev. B* **2002**, *65*, 153401.

[10] I. Popov, S. Gemming, S. Okano, N. Ranjan, G. Seifert, *Nano Lett.* **2008**, *8*, 4093.

[11] K. H. Jin, F. Liu, *Nanoscale* **2020**, *12*, 14661.

[12] C. Shang, L. Fu, S. Zhou, J. Zhao, *JACS Au.* **2021**, *1*, 147.

**ADVANCED
SCIENCE NEWS**

www.advancedsciencenews.com

**ADVANCED
MATERIALS
INTERFACES**

www.advmatinterfaces.de

[13] a) H. Zhu, Q. Wang, C. Zhang, R. Addou, K. Cho, R. M. Wallace, M. J. Kim, *Adv. Mater.* **2017**, *29*, 160624; b) H. Zhu, Q. Wang, L. Cheng, R. Addou, J. Kim, M. J. Kim, R. M. Wallace, *ACS Nano* **2017**, *11*, 11005; c) R. S. Lee, D. Kim, S. A. Pawar, T. Kim, J. C. Shin, S. W. Kang, *ACS Nano* **2019**, *13*, 642; d) H. Kim, J. E. Johns, Y. Yoo, *Small* **2020**, *16*, 2002849; e) H. E. Lim, Y. Nakanishi, Z. Liu, J. Pu, M. Maruyama, T. Endo, C. Ando, H. Shimizu, K. Yanagi, S. Okada, T. Takenobu, Y. Miyata, *Nano Lett.* **2020**, *21*, 243; f) Y. Yoo, J. S. Jeong, R. Ma, S. J. Koester, J. E. Johns, *Chem. Mater.* **2020**, *32*, 9650.